Morpholino, Piperidino, and Pyrrolidino Derivatives of Pyrimidine Nucleosides as Inhibitors of Ribonuclease A: Synthesis, Biochemical, and Crystallographic Evaluation[#,†]

Anirban Samanta,[‡] Demetres D. Leonidas,*[,§] Swagata Dasgupta,*[,‡] Tanmaya Pathak,*[,‡] Spyros E. Zographos,[§] and Nikos G. Oikonomakos[§]

Department of Chemistry, Indian Institute of Technology, Kharagpur 721302, India, and Institute of Organic and Pharmaceutical Chemistry, National Hellenic Research Foundation, 48 Vas. Constantinou Avenue, 11635 Athens, Greece

Received June 16, 2008

Six 5′-deoxy-5′-morpholine, piperidine, and pyrrolidine of pyrimidine nucleosides have been synthesized and characterized. Their inhibitory action to ribonuclease A has been studied by biochemical analysis and X-ray crystallography. These compounds are moderate inhibitors of RNase A with mid-to-upper micromolar inhibition constants (K_i). The high resolution X-ray crystal structures of the RNase A−inhibitor complexes have shown that all inhibitors bind at the enzyme catalytic cleft with the pyrimidine nucleobase at the B_1R_2 subsites while the 5′ group binds away from the main subsite P_1, where $P-O^{5'}$ bond cleavage occurs, toward the solvent close to subsite P_0. Structure−activity relationship analysis has demonstrated that the compounds with the larger group in the 5′ position are more potent. Comparative structural analysis of these RNase A complexes with other similar RNase A−ligand complexes provides a structural explanation of their potency and suggests ways to improve their efficiency and selectivity. These inhibitors can be the starting point for the development of compounds that can be used as pharmaceuticals against pathologies associated with RNase A homologues such as human angiogenin, which is implicated in tumor induced neovascularization.

1. Introduction

Ribonucleases (RNases) are endonucleases that control post-transcriptionally the RNA population in cells. RNases and in particular RNase A,[a] have proven to be excellent model systems for the study of protein structure, folding and stability, and enzyme catalysis. However, during the past decade, members of the RNase A superfamily, the only enzyme family restricted to vertebrates,[1] have also attracted considerable biomedical interest because their biological activities were linked to a variety of malignancies and infectious diseases.[2] Further studies [3−6] have shown that most of these pathological conditions are linked to the ribonucleolytic activity of these proteins, and hence, inhibitors of their enzymatic activity could be potential pharmaceutical agents.[7] The availability of high resolution structures for several members of the RNase A superfamily (human angiogenin, eosinophil ribonucleases) and the wealth of structural information from a large number of inhibitor complexes, particularly with RNase A, have prompted structure assisted drug design efforts to discover potent and selective inhibitors for these enzymes.

Several subsites exist within the central catalytic groove of RNases, where substrate RNA binds. These are defined as $P_0\cdots P_n$, $R_0\cdots R_n$, and $B_0\cdots B_n$ according to the phosphate, ribose, and base of RNA that bind, respectively (n indicates the position of the group with respect to the cleaved phosphate phosphodiester bond where $n = 1$).[8] In all RNases the main subsite P_1 is conserved, whereas subsites B_1 and B_2 on each side of P_1 are partially conserved. Nevertheless, B_1 binds pyrimidines, while B_2 has a strong base preference for purines. Structure-assisted inhibitor design efforts have mainly focused on the parental protein, RNase A, because of the high degree of conservation of the active site among the members of this superfamily and the feasibility for crystallographic studies with this protein. So far the binding of mononucleotide and dinucleotide substrate analogues has been studied,[7,9−11] with the majority of these inhibitors having acidic groups such as phosphate or sulfate.[11,12] All these compounds bind by anchoring their polar phosphate or sulfate group at the central subsite P_1 of the enzyme and are rather moderate inhibitors with dissociation constants in the mid-to-upper micromolar range. The best inhibitor so far is pdUppA-3′p with K_i values of 27 nM, 180 nM, and 360 μM for RNase A, EDN, and angiogenin, respectively,[9,13,14] whereas transition state theory predicts pM values for genuine transition states.[2] However, the major problem associated with these compounds is their transport across the biological membranes. The high negative charge on the phosphate group makes them difficult to use in vivo.[7] More recently aminonucleosides with a carboxylate group have been identified as a new class of inhibitors of RNase A and angiogenin[15] and the binding of the most potent in this series ($K_i = 103\ \mu$M), 3′-*N*-piperidine-4-carboxyl-3′-deoxy-*ara*-uridine (**3Ne**) was studied by X-ray crystallography,[16] revealing a novel ligand-binding pattern.

[#] This paper is dedicated to the memory of our colleague Dr. Nikos G. Oikonomakos.

[†] Atomic coordinates and diffraction data of the RNase A−**U1S**, −**U2S**, −**U3S**, −**U4S**, −**T3S**, and −**T4S** inhibitor complexes have been deposited in the Research Collaboratory for Structural Bioinformatics Protein Data Bank (http://www.rcsb.org) with accession numbers 3D6O, 3D6P, 3D6Q, 3D7B, 3D8Y, and 3D8Z respectively.

* To whom correspondence should be addressed. For D.D.L.: phone, +30 210 7273841; fax, +30 210 7273831; e-mail, ddl@eie.gr. For S.D.: phone, +(091) 3222 283306; fax, +91 3222 255303; e-mail, swagata@iitkgp.ac.in. For T.P.: phone, +(091) 3222 283342; fax, +91 3222 255303; e-mail, tpathak@iitkgp.ac.in.

[‡] Indian Institute of Technology.

[§] National Hellenic Research Foundation.

[a] Abbreviations: RNase A, bovine pancreatic ribonuclease A; EDN, eosinophil derived neurotoxin; 3Ne, 3′-*N*-piperidine-4-carboxyl-3′-deoxy-*ara*-uridine; pdUppA-3′-p, 5′-phospho-2′-deoxyuridine 3-pyrophosphate (P′ → 5′) adenosine 3′-phosphate; PEG, poly(ethylene glycol); araUMP, arabinouridine 3′-phosphate; dUMP, deoxyuridine 3′-phosphate; **U1S**, 5′-deoxy-5′-*N*-(ethyl isonipecotatyl)uridine; **U2S**, 5′-deoxy-5′-*N*-morpholinouridine; **U3S**, 5′-deoxy-5′-*N*-piperidinouridine; **U4S**, 5′-deoxy-5′-*N*-pyrrolidinouridine; **T3S**, 5′-deoxy-5′-*N*-piperidinothymidine; **T4S**, 5′-deoxy-5′-*N*-pyrrolidinothymidine.

10.1021/jm800724t CCC: $40.75
Published on Web 01/27/2009

Scheme 1. Synthesis of 5′-Deoxy-5′-alkylaminouridine Derivatives[a]

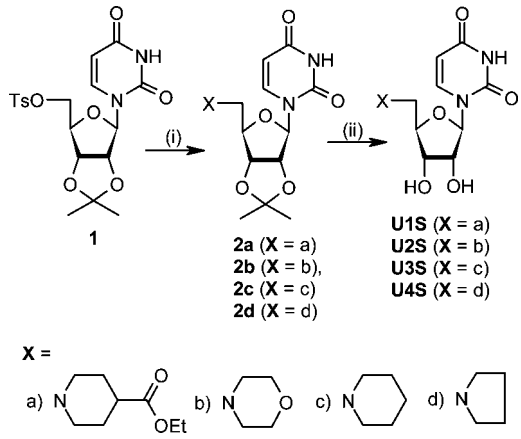

[a] Reagents and conditions: (i) **2a**, ethyl isonipecotate, 60 °C, 24 h (63%); **2b**, morpholine, 60 °C, 55 h (78%); **2c**, piperidine, 60 °C, 48 h (82%); **2d**, pyrrolidine, room temp, 5 h, and then 60 °C, 41 h (72%); (ii) TFA/H_2O (7/3, v/v), room temp, 30 min, **U1S** (67%), **U2S** (65%), **U3S** (69%), **U4S** (66%).

Scheme 2. Synthesis of 5′-Deoxy-5′-alkylaminothymidine Derivatives[a]

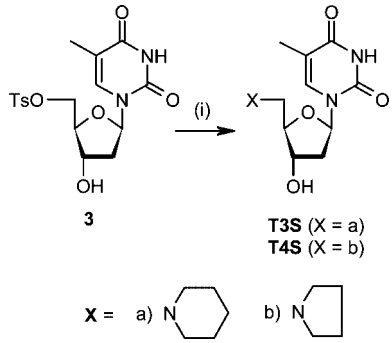

[a] Reagents and conditions: (i) **T3S**, piperidine, 60 °C, 26 h (76%); **T4S**, pyrrolidine, 60 °C, 22 h (81%).

The polarity of all these compounds may hinder their potential pharmaceutical use, since it may impede their cell permeability and bioavailability. Hence, we have turned our attention toward less polar compounds and we have synthesized and studied the binding of a series of uridine and thymidine analogues that have a morpholino, piperidino, or pyrrolidino group at the 5′ position. Here, we present the synthesis, kinetic evaluation, and the high resolution crystal structures of the RNase A in complex with six compounds from this series. Their inhibitory potency is moderate, and their binding mode reveals that polar acidic groups are not necessary for the anchorage of the inhibitor in the active site. Furthermore, it seems that the 5′ groups have a significant role in the potency of these inhibitors. This evidence can be the starting point for further design, since it indicates ways for improving their selectivity and efficiency.

2. Results and Discussion

2.1. Chemistry. The synthetic routes toward the 5′-deoxy-5′-alkylaminouridine derivatives **U1S**−**U4S** and 5′-deoxy-5′-alkylaminothymidine derivatives **T3S** and **T4S** are outlined in Schemes 1 and 2, respectively.

2.2. Biology. The inhibitory activity of the synthesized compounds against RNase A was initially studied by the agarose gel-based assay (Figure 1a). Lane 1 of the gel shows the most intensity because of the presence of only control tRNA. As a result of the degradation of tRNA by RNase A, lane 2 has the least intensity. Lanes 3−5 of each gel contain tRNA and RNase A with increasing concentration of synthesized compounds **U1S**−**U4S** and **T3S** and **T4S** individually. The difference in intensity between lane 2 and lane 3 is maximum for compound **U1S**, and these differences gradually increase in lanes 4 and 5. The other uridine derivatives **U2S**, **U3S**, and **U4S** also exhibit some inhibitory activity as observed qualitatively, while the thymidine derivatives **T3S** and **T4S** show less activity. In a comparative agarose gel with equimolar concentrations of the compounds, the uridine analogue shows better activity than the thymidine analogue (Figure 1b).

The ribonucleolytic activity of the compounds was further assessed by the precipitation assay (Figure 2). The percent reduction of the ribonucleolytic activity of all compounds for RNase A at the same concentration (0.32 mM) was compared. The activity of RNase A is reduced by 30% by compound **U1S**, while values for **U2S**, **U3S**, and **U4S** range from 17% to 12%. Compounds **T3S** and **T4S** show little inhibitory activity (reduction of ribonucleolytic activity around 5%).

For determination of the inhibition constants by kinetic experiments, the reciprocal of reaction velocity has been plotted against inhibitor concentration for three different substrate concentrations (Figure 3). The linear Dixon plot for the three different concentrations of the same substrate intersects at an inhibitor concentration equal to the negative reciprocal of the inhibitor association constant. The plots of compound **U1S** and **U2S** are given in parts A and B of Figure 3, respectively, while those of compounds **U3S**, **U4S**, **T3S**, and **T4S** are given in the Supporting Information. The nature of the plots is indicative of competitive inhibition.

The chemical structure and the inhibition constant values of the RNase A enzyme for the six compounds are shown in Table 1. Compound **U1S** is the most potent of the six compounds, and **T3S** and **T4S** are the least potent.

2.3. X-ray Crystallography. To elucidate the structural basis of inhibition, we have determined the crystal structure of RNase A in complex with **U1S**, **U2S**, **U3S**, **U4S**, **T3S**, and **T4S**. The crystallographic asymmetric unit of the monoclinic RNase A crystals used in this study contains two protein molecules (A and B).[16] However, inhibitor molecules were found bound only in molecule A of the noncrystallographic RNase A dimer. This partial binding has also been observed in previous crystallographic studies with the same monoclinic crystals of RNase A [10,16−18] and might be attributed to the crystal lattice that impedes access to the active site of molecule B in the asymmetric unit. This phenomenon provided us with two structures (one free and one inhibitor complexed) from the same crystal, thus facilitating a comparative structural analysis of the binding of each ligand to RNase A.

Upon binding to RNase A, each of the inhibitor displaces five water molecules from the active site of the free enzyme. There are no significant conformational changes in the catalytic site of RNase A upon ligand binding. The rms distances between the structures of free RNase A[16] and those of the **U1S**−, **U2S**−, **U3S**−, **U4S**−, **T3S**−, and **T4S**−RNase A complexes are 0.13, 0.20, 0.15, 042, 0.21, and 0.21 Å for the Cα atoms for 124 equivalent protein residues, respectively. The rms deviation of the Cα positions between all six complexes ranges between 0.2 and 0.5 Å, revealing that the structural differences between the six complex structures are very small. These are mainly concentrated on the loop regions and are not related to the binding of the different inhibitors.

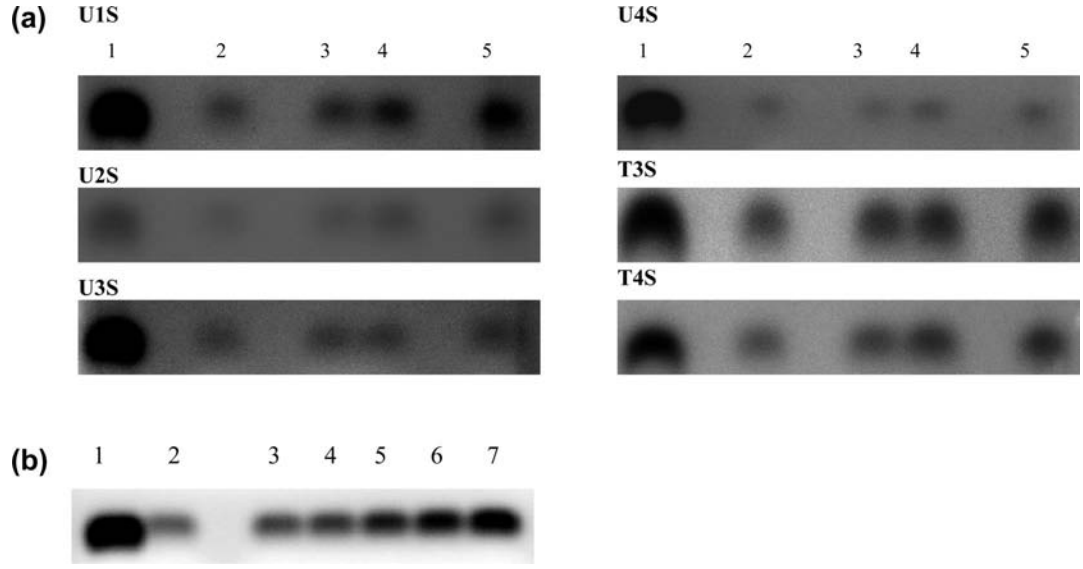

Figure 1. (a) Agarose gel based assay for the inhibition of RNase A: (lane1) tRNA; (lane 2) tRNA and RNase A (1.37 μM); (lanes 3, 4, and 5) tRNA, RNase A and **U1S**−**U4S** (0.10, 0.21, and 0.31 mM, respectively), and **T3S** and **T4S** (0.13, 0.27, 0.40 mM), respectively. (b) Comparative agarose gel based assay for the inhibition of RNase A: (lane 1) tRNA; (lane 2) tRNA and RNase A (1.26 μM); (lanes 3, 4, 5, 6, and 7) tRNA, RNase A with **T4S**, **T3S**, **U4S**, **U3S**, and **U2S**, respectively (compound concentrations 0.14 mM).

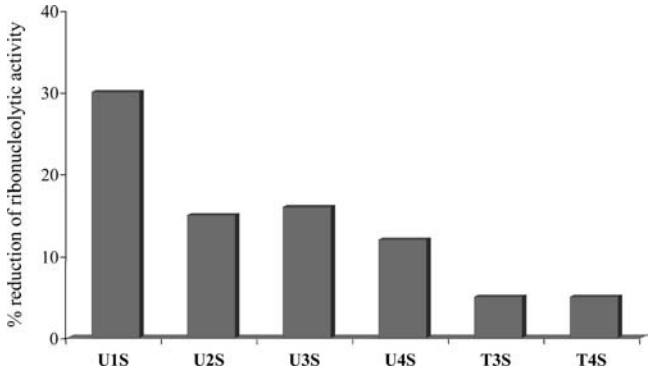

Figure 2. Reduction of ribonucleolytic activity of RNase A (1.10 μM) in the presence of compounds **U1S**−**U4S**, **T3S**, and **T4S** (0.32 mM each) by RNA precipitation assay.

The structures of the **U1S**, **U2S**, **U3S**, and **U4S** complexes are defined at 1.6 Å resolution and contain 329, 312, 378, and 348 water molecules, respectively. The structures of the **T3S** and **T4S** complexes are determined at a slightly lower resolution (1.7 and 2.0 Å) and contain 213 and 166 water molecules, respectively. In addition, complexes **U3S**, **U4S**, and **T3S** contain two citrate molecules from the crystallization media while complex **T4S** contains one. Numbering scheme definitions for **U2S** and **T3S** are presented in Figure 9, and the same definition was used for the rest of the inhibitors.

All atoms of the six inhibitor molecules are well defined within the sigmaA weighted $2F_o - F_c$ electron density map of the RNase A complexes (Figure 4). The only exception is inhibitor **U1S** where there is no sufficient electron density for the carboxyethyl group, and hence, this part of the inhibitor was not included in the model. The 5′-morpholino, piperidino, or pyrrolidino group has higher temperature factors than the rest of the molecule and appears to be more mobile. Upon binding to RNase A, all inhibitor molecules adopt similar conformations. The glycosyl torsion angle χ adopts the frequently observed[19] anti conformation. The ribose adopts the quite rare C4′-exo puckering in the uridine derivatives, while in the thymidine analogues **T3S** and **T4S** are found in the C2′-exo and O4′-exo conformations, respectively. The rest of the backbone torsion angles are in the common range for protein bound pyrimidines.[19] The morpholino, piperidino, and pyrrolidino moieties adopt the chair conformation, whereas the five-membered pyrrolidine ring adopts an envelope conformation (Figure 5).

The anchoring point for all six inhibitors is the pyrimidine base which binds at subsite B_1 in the same manner as previous pyrimidine inhibitors (Figure 5). Subsite B_1 is a pocket formed by His12, Val43, Asn44, Thr45, Phe120, and Ser123. The primary functional component of this subsite is Thr45, which forms two hydrogen bonds with pyrimidine: its main-chain NH donates a hydrogen to O2 of the uracil or thymine, and its Oγ1 donates a hydrogen to N3 of thymine or uracil (Figure 6). In all six crystal structures of RNase A complexes the Thr45 side chain also hydrogen-bonds with the carboxylate of Asp83 like in previous RNase A−uridine complexes.[20] Ser123 Oγ forms a water-mediated hydrogen bond with O4 as in previous RNase A complexes.[21−23] The phenyl group of Phe120 sits on one side of the pyrimidine ring near O2, making van der Waals contacts. His12 Cε1 also contacts O2 on the same side of the ring. Val43 and Asn44 occupy the space on the opposite side, the main-chain carbonyl and α carbon of Asn44 contact O2, whereas the side chain atoms of Val43 lie in van der Waals contact distance from the pyrimidine ring. The ribose binds at subsite R_2, and it is held in place by hydrogen bond interactions of its hydroxyl groups with the side chain atoms of Lys41 and His119 and by participating in an extended water-mediated hydrogen-bonding network along with the protein (Table 2). The 5′-substituent group is pointing toward the solvent in a location close to but not at subsite P_0, adopting a conformation imposed probably by the stereochemistry of the ligand (Figure 6).

In all free RNase A structures reported so far the side chain of the catalytic residue His119 adopts two conformations, denoted as productive ($\chi_1 \approx 160°$) and nonproductive ($\chi_1 \approx -80°$), which are related by a 100° rotation about the Cα−Cβ bond and a 180° rotation about the Cβ−Cγ bond.[16,24−27] These conformations are dependent on the pH[28] and the ionic strength

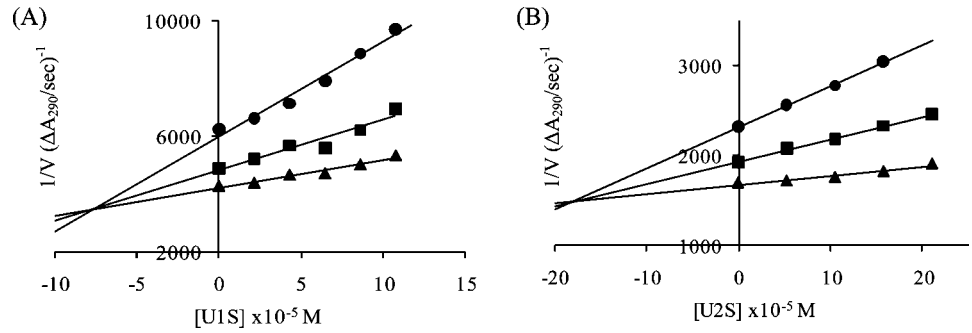

Figure 3. Dixon plots for inhibition of RNase A by (A) **U1S** (0−0.108 mM), 2′,3′-cCMP concentrations of 0.061 (●), 0.091 (■), 0.122 mM (▲), and RNase A concentration of 0.83 μM. (B) **U2S** (0−0.211 mM), 2′,3′-cCMP concentrations of 0.135 (●) and 0.203 (■) and RNase A concentration of 1.08 μM. Calculated K_i values are listed in Table 1.

Table 1. Structures and Kinetic Parameters (from the Dixon Plot) of the Inhibitors

Inhibitor molecule	Structure	K_i (μM)
U1S	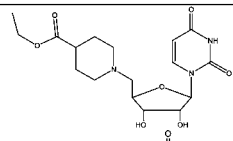	77±1
U2S	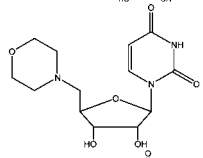	179±3
U3S	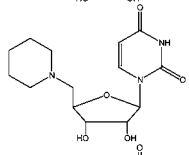	172±4
U4S	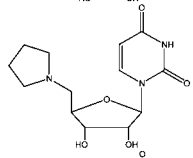	203±1
T3S	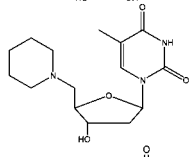	396±2
T4S	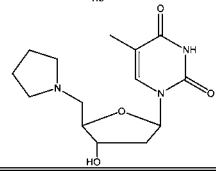	423±6

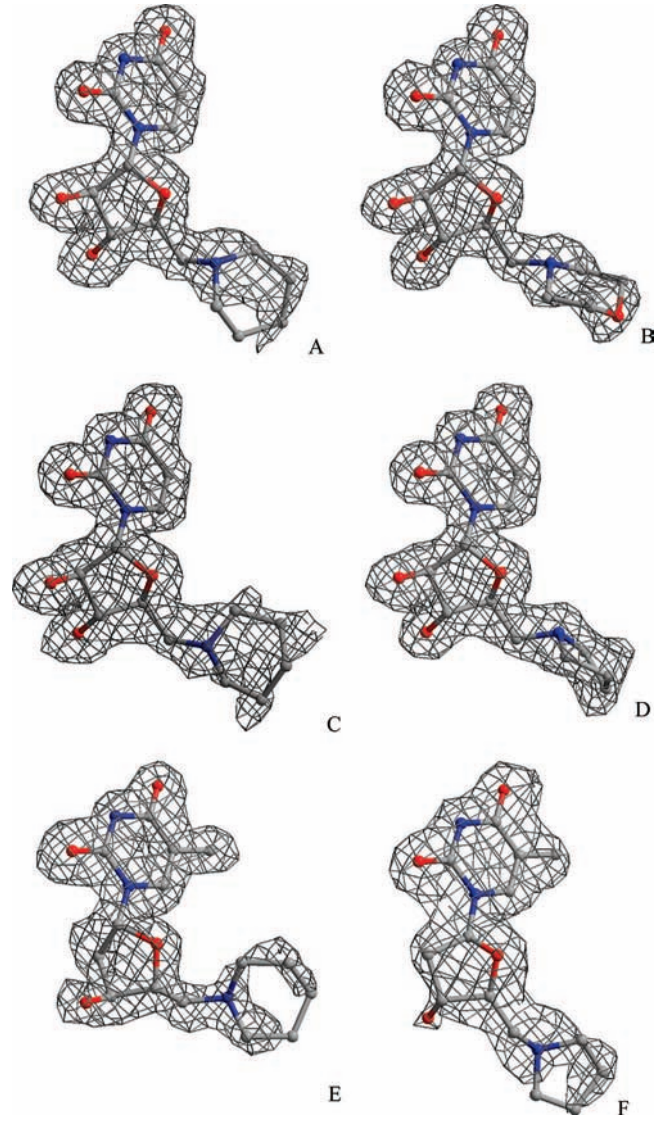

Figure 4. Diagrams of the sigmaA $2|F_o| - |F_c|$ electron density maps calculated from the RNase A model before incorporating the coordinates of each ligand, contoured at 1.0σ level. The refined structures of the inhibitor are shown as ball-and-stick models for molecules **U1S** (A), **U2S** (B), **U3S** (C), **U4S** (D), **T3S** (E), and **T5S** (F).

of the crystallization solution.[29] Previous studies[21] have shown that binding of ligand groups in P_1 induces the productive conformation of the side chain of His119. In complexes **U1S**, **U3S**, **U4S**, and **T4S** the side chain of His119 is found in both alternative conformations, while in complexes **U2S** and **T3S** the side chain adopts the nonproductive conformation. These observations are consistent with the binding of the inhibitors away from subsite P_1.

Upon binding to RNase A, inhibitor molecules become partly buried. The solvent accessibilities of the free ligand molecules **U1S**, **U2S**, **U3S**, **U4S**, **T3S**, and **T4S** are 483, 477, 479, 465, 488, and 490 Å^2, respectively. When bound, these molecular surfaces shrink to 241, 233, 241, 222, 241, and 225 Å^2, respectively. This indicates that approximately 50% of the surfaces of the ligand molecules become buried. Compounds **U1S**, **U2S**, and **U4S** on binding to RNase A make a total of 5 hydrogen bonds and 17 van der Waals interactions (**U1S**, 7 nonpolar/nonpolar, 10 polar/nonpolar; **U2S**, 5 nonpolar/nonpolar, 12 polar/nonpolar; **U4S**, 6 nonpolar/nonpolar, 11 polar/nonpo-

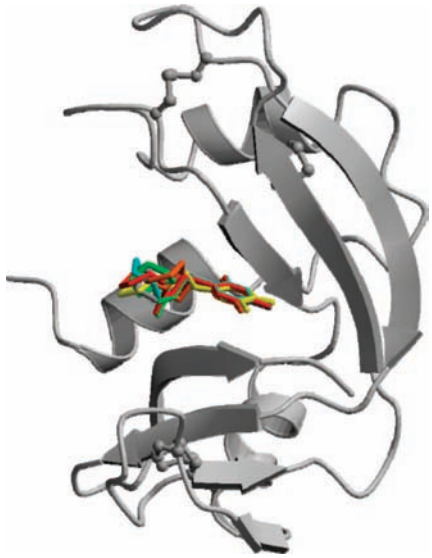

Figure 5. Schematic diagram of the RNase A molecule with the superimposed structures of the six inhibitor molecules bound. Coloring scheme used is as follows: **U1S**, red; **U2S**, cyan; **U3S**, green; **U4S**, gray; **T3S**, orange; **T4S**, yellow.

lar). **U3S** makes a total of 6 hydrogen bonds and 20 van der Waals interactions (9 nonpolar/nonpolar and 11 polar/nonpolar). **T3S** and **T4S** make a total of 3 hydrogen bonds and 19 and 15 van der Waals interactions, respectively (**T3S**, 8 nonpolar/nonpolar, 11 polar/nonpolar; **T4S**, 5 nonpolar/nonpolar, 10 polar/nonpolar). van der Waals interactions of the six ligands are presented in Table 3.

Although the structures presented here are based on soaking experiments, data from RNase A cocrystallized with 5 mM of each inhibitor were also available at 2.0 Å resolution. Crystallographic analysis of these structures showed that all inhibitors were bound in exactly the same way as in the soaked crystals.

2.4. SAR Analysis. The kinetic results are summarized in Table 1. It seems that the diversity of structural skeleton of the 5′-group has an impact on RNase A inhibition, since the potency of the six compounds ranges from 77 to 423 μM. Earlier kinetic studies[13,30,31] had demonstrated that thymidine nucleotides bind to RNase A with K_i values comparable with those of uridine inhibitors. However, the uridine compounds tested in this work are more potent than the thymidine ones. This can be attributed to the interactions of the 2′-hydroxyl group of the ribose with RNase A residues in the uridine compounds which are not possible with the thymidine compounds since these lack this group. The 2′-hydroxyl group participates in hydrogen-bond interactions with the side chain atoms of P_1 residues His12 and Lys41 (Table 2). Furthermore, they are also involved in water-mediated interactions with His119 and Phe120 (Table 2) and van der Waals interactions with His12 and Lys41 (Table 3). These interactions are important for RNase catalysis and cannot be observed in most substrate analogues, which are frequently deoxynucleotides. Furthermore, it seems that the potency of the uridine inhibitors increases with the size of the 5′-substituent with **U1S** which has the largest group, being the most potent of all six inhibitors, while **U2S** and **U3S** with 5′-groups of similar size are almost equipotent. Similarly, **T3S** is slightly more potent than **T4S**, which has a slightly smaller 5′-group (one atom difference). Therefore, it seems that despite the fact that the 5′-group does not participate in any direct hydrogen-bond interactions with the protein in any of the six inhibitors, it has a significant contribution to the potency of the inhibitor. In complexes **U1S**−**U4S** and **T4S** the 5′-group does not participate in any van der Waals interactions with protein residues either (Table 3). In contrast, in the thymidine complex with **T3S**, this group is involved in van der Waals interactions with Val43 (Table 3). **U1S** has a more polar group at the 5′ position than the other five ligands, and although its position is not defined in the electron density map, we cannot rule out that it may also affect its capacity.

2.5. Comparative Structural Analysis. The B_1 subsite has been shown to exhibit a strong base preference for pyrimidines,[32] and the interactions of pyrimidine bases in this site have been examined by crystallography or NMR [complexes with d(CpA),[23,33] UpcA,[22,34] 2′,5′-CpA,[33,35] U3′p, U2′p,[10] 3′CMP,[23] araUMP,[11] dUppA-3′-p,[36] pdUppA-3′-p,[14] pTppA-3′p,[37] and N3e [16]]. From the kinetic constants it seems that all six inhibitors are moderate inhibitors of RNase A and the uridine inhibitors (**U1S**−**U4S**) have similar potency to the 3′-*N*-alkylamino-3′-deoxy-*ara*-uridines ($K_i = 103$ μM for the best inhibitor **3Ne** of this family)[15] and to 3′CMP ($K_i = 103$ μM)[38] but much lower than that of araUMP ($K_i = 6$ μM)[11] and pTppA-3′p ($K_i = 0.041$ μM).[13] Like the alkylamino-*ara*-uridines they also lack a phosphate or a sulfate group. Structural comparison of the binding of the pyrimidine derivatives presented in this study to the binding of araUMP to RNase A[11] and to that of 3′CMP[38] shows that the pyrimidine bases and the ribose of the inhibitors superimpose well while the 5′ groups do not superimpose onto the phosphate group of araUMP or 3′CMP which binds at subsite P_1 (parts c and d of Figure 7). Both 3′CMP and araUMP exploit interactions with subsite P_1 through their phosphate group which cannot be utilized by the pyrimidine compounds we studied, since they lack such a group. The weaker binding of our compounds compared to araUMP could be attributed to the phosphate interactions of araUMP with residues in subsite P_1 which our compounds does not exploit. On the basis of the similar potency of our compound and 3′CMP, it seems that the binding of the uracil or thymine to subsite B_1 is stronger than the cytosine binding at this subsite. Although a comparison of k_{cat}/K_m values for cytidylyl and uridylyl substrates[9,32] shows that the B_1 site of RNase A has a small preference for cytosine over uracil, mutational studies by delCardayre and Raines[39,40] have shown that the hydrogen bond between the pyrimidine N3 and Thr45 Oγ1 in RNase A favors uracil over cytosine. The two key findings in these studies were as follows: (i) substitution of Ala for Asp83 decreases activity toward uridylyl nucleotides by 10-fold but barely affects cleavage of cytidylyl substrates and (ii) replacement of Thr45 by Gly in D83A-RNase lowers activity toward uridylyl and cytidylyl substrates similarly, by 11-fold and 6-fold, respectively. These results suggested that the observed hydrogen bond between Thr45 Oγ1 and N3 of the pyrimidine ring is functionally important and that its strength is modulated by the additional interaction of the threonine side chain with Oδ of Asp83. In the absence of Asp83, the hydrogen bonds with N3 of cytosine and uracil are nearly comparable in avidity; Asp83 selectively improves the interaction with uracil, probably by increasing the partial negative charge on Thr45 Oγ1 and by aligning the hydroxyl appropriately. This preference together with the hydrogen-bond interactions of the 3′-hydroxyl group of our compounds compensates for the hydrogen bond interactions between the 3′-phosphate group of 3′CMP and RNase A residues in subsite P_1.

U-2′-p and U-3′-p are more potent inhibitors of RNase A with K_i values of 7.1 and 82 μM, respectively,[38] than the four uridine inhibitors presented in this study. Structural superposition of the four RNase A−uridine inhibitor complexes onto the U-2′-p and U-3′-p complexes reveals that the uridine moiety of

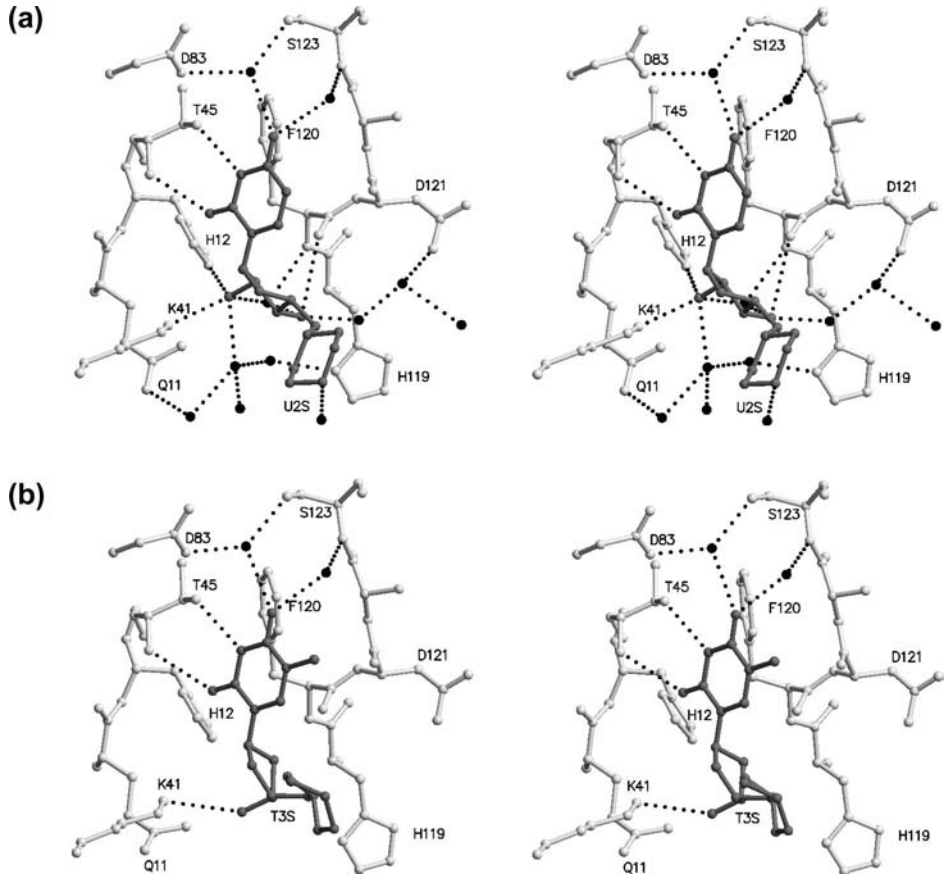

Figure 6. Stereodiagrams of the interactions between RNase A and molecules **U2S** (a) and **T3S** (b). The side chains of protein residues involved in ligand binding are shown as ball-and-stick models. Bound waters are shown as black spheres. Hydrogen bond interactions are represented as dashed lines.

Table 2. Potential Hydrogen Bond Interactions of the Inhibitors When Bound to RNase A in the Crystal[a]

		distance (Å)					
inhibitor atoms	RNase A atoms	**U1S**	**U2S**	**U3S**	**U4S**	**T3S**	**T4S**
O2′	His12 Nε2	3.2	3.2	3.4	3.2		
O2′	Lys41 Nζ	2.7	2.7	2.9	2.9		
O2	Thr45 N	2.9	2.9	0.9	2.9	3.0	3.0
N3	Thr45 Oγ	2.7	2.7	2.7	2.7	2.8	2.7
O3′	Lys41 Nζ					2.8	
O3′	His119 Nδ1	2.8		2.5	2.6		3.3
O3′	Phe120 O		3.4	3.4			
O2′	Wat1	3.0	2.9				
O3′	Wat8						2.7
O3′	Wat38	3.2	3.0	3.1	3.0		
O2′	Wat38	3.0	3.0	3.2	3.2		3.2
O4	Wat102	3.1	3.0	2.9	2.9	2.9	3.2
O4	Wat194	2.8	2.8	2.8	2.8	2.9	2.6
O3′	Wat303		2.4				
OAM	Wat309		3.1				
NAU	Wat2			3.4			
O4′	Wat7					3.4	

[a] Hydrogen bond interactions were calculated with the program HB-PLUS.[56] For ligand atom definitions, see Figure 9. Water mediated interactions: Wat1 is hydrogen-bonded to Wat268, Wat319, and Wat321. Wat268 is hydrogen-bonded to His119 Nδ1, and Wat321 is hydrogen-bonded to Gln11 Oε1. Wat8 is hydrogen-bonded to His119 Nδ1. Wat38 forms hydrogen bonds with His119 Nε2 and Phe120 N. Wat102 is hydrogen-bonded to Ser123 N. Wat194 is hydrogen-bonded to Asp83 Oδ1 and to Ser123 Oγ. Wat303 is hydrogen-bonded to Wat302, and this is hydrogen-bonded to Asp121 Oδ1 and to Wat22.

all inhibitors superimposes well inside the catalytic cleft of the enzyme. However, while the phosphate groups of U-2′-p and U-3′-p bind at subsite P_1 engaging in hydrogen bond interactions with RNase A residue His119, the 5′-group of **U1S**, **U2S**, **U3S**, and **U4S** is bound away from the catalytic cleft toward the solvent. This results in the loss of the hydrogen interactions with His119 and a decrease in the potency of inhibitors **U1S**, **U2S**, **U3S**, and **U4S**.

The structure of the RNase A−**3Ne** complex in RNase A revealed two inhibitor molecules bound in the central RNA binding cavity of RNase A exploiting interactions with residues from peripheral binding sites rather than from the active site of the enzyme.[16] In the RNase A−**3Ne** complex, one of the inhibitor molecules is bound with its carboxylate group at subsite B_1, and it was postulated that the carboxylate imitates the carbonyl groups of uracil.[16] Structural superposition of our RNase A−inhibitor complexes onto the RNase A−**3Ne** complex (Figure 7b) shows that uracil or thymine superimposes onto the carboxylate group of one of the two **3Ne** molecules in the active site. Unlike in the **3Ne** complex none of the 5′-group of ligands **U1S**−**U4S**, **T3S**, and **T4S** can imitate the carbonyl groups of uracil or thymine, and hence, the binding mode of these morpholino, piperidino, and pyrrolidino nucleotides follows a more rational pattern (i.e., the nucleotide base, uracil, or thymine binds at subsite B_1 and the 3′-hydroxyl group interacts with residues from subsite P_1) in comparison to the **3Ne** binding pattern.

Structural superposition of each of the RNase A uridine or thymidine complexes onto the RNase A−pdUppA-3′-p and the RNase A−pTppA-3′-p complexes reveals that the uridine or thymidine part of the inhibitors superimposes onto the uridine part of pdUppA-3′-p and the thymidine part of pTppA-3′-p while the 5′-morpholino, piperidino, or pyrrolidino group is close to

Table 3. Potential van der Waals Interactions of Ligands **U1S**−**U4S**, **T3S**, and **T4S** upon Binding to RNase A[a]

	ribonuclease A atoms (molecule A)					
inhibitor atom	**U1S**	**U2S**	**U3S**	**U4S**	**T3S**	**T4S**
C3′	His119 Cε1		His119 Cε1			
O4′					Val43 Cγ2	Val43 Cγ2
O3′	His119 Cε1		His119 Cδ2	His119 Cδ2	Lys41 Cε	His119 Cδ2
C2′	His12 Cε1; Phe120 O	His12 Cε1; Phe120 O	His12 Cε1; Phe120 O	His12 Cε1; Phe120 O	Phe120 O	His12 Cε1; Lys41 Nζ
O2′	His12 Cε1; Lys41 Cε	His12 Cε1; Lys41 Cε	His12 Cε1; Lys41 Cε	His12 Cε1; Lys41 Cε		
C1′	Val43 O	Val43 O	Val43 O	Val43 O	Val43 Cγ2	
C6			Val43 Cγ1	Val43 Cγ1	Val43 Cγ2	Val43 Cγ2
C5			Val43 Cγ1			
CM					Lys66 Nζ; Asp121 O	Lys66 Nζ
C4	Phe120 Cε2, Cδ2	Thr45 Oγ1; Phe120 Cε2, Cδ2	Phe120 Cε2, Cδ2	Phe120 Cε2, Cδ2	Phe120 Cε2, Cδ2	Phe120 Cε2, Cδ2
N3	Thr45 Cβ; Phe120 Cε2, Cδ2	Thr45 Cβ; Phe120 Cε2, Cδ2	Thr45 Cβ; Phe120 Cε2, Cδ2	Thr45 Cβ; Phe120 Cε2, Cδ2	Thr45 Cβ; Phe120 Cε2, Cδ2	Thr45 Cβ; Phe120 Cε2, Cδ2
C2	Asn44 Cα; Phe120 Cδ2	Asn44 Cα; Thr45 N; Phe120 Cδ2	Val43 Cγ1; Asn44 Cα; Phe120 Cδ2	Asn44 Cα; Phe120 Cδ2	Asn44 Cα; Phe120 Cδ2	Phe120 Cδ2
O2	His12 Cε1; Asn44 Cα, C	His12 Cε1; Asn44 Cα, C	His12 Cε1; Asn44 Cα, C	His12 Cε1; Asn44 Cα, C	His12 Cε1; Asn44 Cα, C	His12 Cε1; Asn44 Cα
CAH					Val43 Cγ2	
CAJ					Val43 Cγ2	
total	17 contacts (7 residues)	17 contacts (6 residues)	20 contacts (7 residues)	17 contacts (7 residues)	19 contacts (8 residues)	14 contacts (9 residues)

[a] For ligand atom definitions, see Figure 9.

the position occupied by the 5′-phosphate group of pdUppA-3′-p (Figure 7a) or pTppA-3′-p (Figure 8).

3. Conclusion

A new class of non-natural 5′-nucleotides has been identified as RNase A inhibitors. These compounds have a morpholino, piperidino, or pyrrolidino group at the 5′-position and are moderate inhibitors of RNase A. The structural basis of their inhibition has been revealed by X-ray crystallography at high resolution. All inhibitor molecules bind to RNase A with their uridine or thymidine moiety in subsites B_1R_2, while the rest of the molecule projects to the solvent close to P_0. This was not anticipated, since there is no obvious reason for why the binding of these inhibitors does not follow the binding pattern of similar pyrimidine nucleotides to place the 5′ morpholino, piperidino, or pyrrolidino group at subsite P_1, but instead it binds away from it. This observation shows that even small modifications of the inhibitor's chemical structure can generate profound alterations in its mode of interaction with the target protein. These findings also emphasize the importance of obtaining direct structural information on each new inhibitor complex on the optimization pathway.

Structure assisted design for new inhibitors requires detailed knowledge of the protein−ligand interactions and a significant number of protein−ligand complex structures. Thus, any new structural data on complexes between RNase A and substrate analogues are of important use for a better understanding of inhibitor binding and enzyme catalytic mechanism. Comparative structural analysis of the RNase A in complex with **U1S**, **U2S**, **U3S**, **U4S**, **T3S**, and **T4S**, with other RNase A−ligand complexes (**3Ne**), suggests ways to improve their potency, and this study could be the starting point for the design of better inhibitors. Thus, we propose adding a suitably longer group at the 3′-hydroxyl group of the ribose moiety of **U1S**, **U2S**, **U3S**, **U4S**, **T3S**, and **T4S** that can form additional interactions with residues at subsite B_2, yielding a much more potent inhibitor.

4. Experimental Section

4.1. Chemistry. Materials and General Methods. Ethyl isonipecotate was purchased from Sigma-Aldrich, and all other reagents were from SRL India. Column chromatographic separations were done using silica gel (60−120 and 230−400 mesh). Solvents were dried and distilled following standard procedures. TLC was carried out on precoated plates (Merck silica gel 60, f_{254}), and the spots were visualized with UV light or by charring the plates dipped in 5% H_2SO_4−MeOH solution or 5% H_2SO_4/vanillin/EtOH or 5% ninhydrin in MeOH solution. ^{1}H NMR (400 MHz) and ^{13}C NMR (100 MHz) spectra were recorded on Bruker NMR instrument. All ^{1}H NMR in D_2O were recorded using CH_3CN as internal standard. All ^{13}C NMR in D_2O were recorded using DMSO-d_6 as internal standard. Chemical shifts are reported in parts per million (ppm, δ scale).

5′-Deoxy-5′-*N*-(ethyl isonipecotatyl)uridine U1S. A mixture of 5′-*O*-tosyl-2′,3′-*O*-isopropylidineuridine **1**[41] (1.50 g, 3.42 mmol) and ethyl isonipecotate (12 mL) was heated at 60 °C. After 24 h, the reaction mixture was cooled to room temperature and diluted with EtOAc (50 mL). The EtOAc solution was washed with water (3 × 20 mL), separated, dried over anhydrous Na_2SO_4, and filtered. The filtrate was evaporated to dryness and the solid residue was purified over a silica gel column to afford compound **2a** (0.91 g, 63%). Compound **2a** (0.20 g, 0.47 mmol) was stirred with 70% trifluoroacetic acid in water (5 mL) at room temperature. After 3 h, the solvent was evaporated to dryness under reduced pressure and coevaporated with ethanol (2 × 5 mL). The residue was purified over a silica gel column by using $CHCl_3$ and MeOH solvent to obtain compound **U1S** (0.11 g, 57%). Hygroscopic solid. ^{1}H NMR (D_2O): δ 1.25 (t, J = 7.2 Hz, 3H), 1.69−1.78 (m, 2H), 1.96−1.99 (m, 2H), 2.43−2.53 (m, 3H), 2.83−2.96 (m, 2H), 3.08 (bs, 2H), 3.99−4.03 (m, 1H), 4.14−4.24 (m, 3H), 4.32 (bs, 1H), 5.78 (s, 1H), 5.86 (d, J = 8 Hz, 1H), 7.65 (d, J = 8 Hz, 1H). HRMS (ES$^+$), m/z calculated for $(M + H)^+$ $C_{17}H_{26}N_3O_7$, 384.1771; found, 384.1775.

5′-Deoxy-5′-*N*-morpholinouridine U2S. This compound was prepared according to the method discussed for compound **U1S**. The reaction between compound **1** (0.45 g, 1.03 mmol) and morpholine (4 mL) at 60 °C for 55 h afforded compound **2b** (0.28 g, 78%). Compound **2b** (0.20 g, 0.57 mmol) was converted to compound **U2S** (0.12 g, 65%) in 3 h. Hygroscopic solid. ^{1}H NMR (D_2O): δ 2.66 (bs, 4H), 2.75−2.86 (m, 2H), 3.76 (bs, 4H), 3.99−4.03 (m, 1H), 4.19−4.23 (m, 1H), 4.31 (bs, 1H), 5.79 (s, 1H), 5.87 (d, J = 8 Hz, 1H), 7.67 (d, J = 8 Hz, 1H). HRMS (ES$^+$), m/z calculated for $(M + H)^+$ $C_{13}H_{20}N_3O_6$, 314.1352; found, 314.1353.

Compounds **U3S** and **U4S** were synthesized according to the method discussed for compound **U1S**. Compounds **T3S** and **T4S**

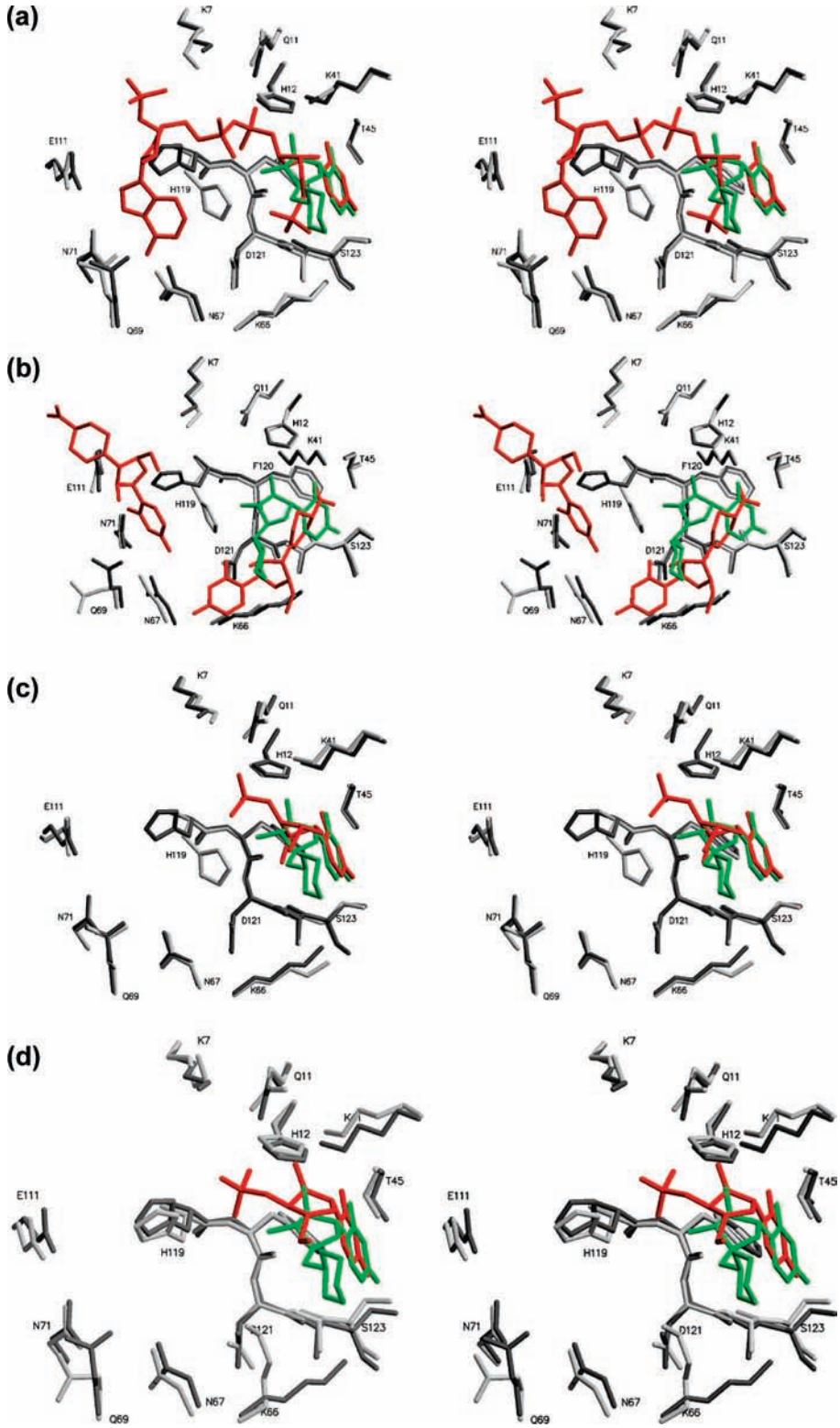

Figure 7. Stereodiagram of the structural comparisons of the RNase A−**U2S** (gray) complex and complexes RNase A−pdUppA-3′p (a), RNase A−**3Ne** (b), RNase A−araUMP (c), and RNase A−3′CMP (d). Ligand molecules are shown in color: **U2S** in green; pdUppA-3′p, **3Ne**, araUMP, 3′CMP, and pTppA-3′-p in red. Protein residues are also shown.

were synthesized from 5′-*O*-tosylthymidine **3**[42] following a procedure[43] reported earlier. For details see Supporting Information.

4.2. Enzymatic Assays. Bovine pancreatic RNase A, yeast tRNA, 2′,3′-cCMP, 3′-CMP, and human serum albumin (HSA) were purchased from Sigma-Aldrich. UV−vis measurements were made using a Perkin-Elmer UV−vis spectrophotometer (model Lambda 25). Concentrations of the solutions were determined spectrophotometrically using the following data: $\varepsilon_{278.5} = 9800\ M^{-1}\ cm^{-1}$ (RNase A)[44] and $\varepsilon_{268} = 8500\ M^{-1}\ cm^{-1}$ (2′,3′-cCMP).

(A) Agarose Gel-Based Assay. (i) Inhibition of RNase A was assayed qualitatively by the degradation of tRNA in an agarose gel. In this method, 20 μL of RNase A (stock concentration 6.87 μM) was mixed with 20, 40, and 60 μL of the compounds **U1S**−**U4S** (stock concentration 0.52 mM) and **T3S** and **T4S** (stock

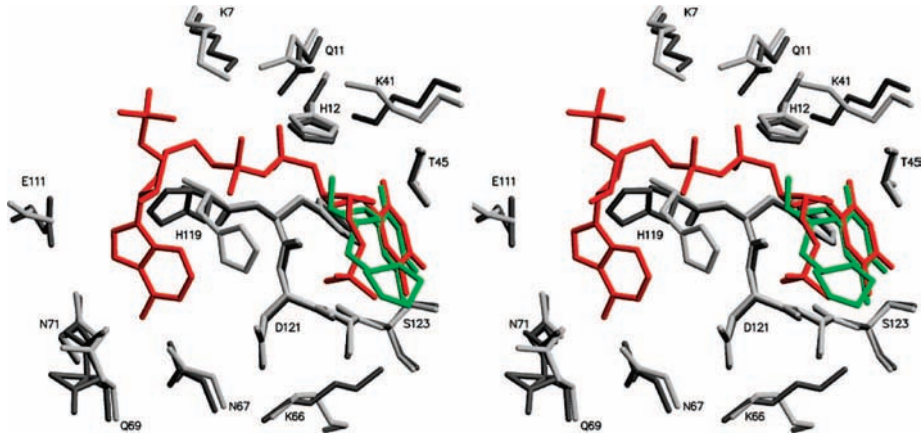

Figure 8. Stereodiagram of the RNase A−**T3S** complex structure (gray) superimposed onto the RNase A−pTppA-3′-p complex structure (white). Ligand molecules **T3S** and pTppA-3′-p are in green and red, respectively.

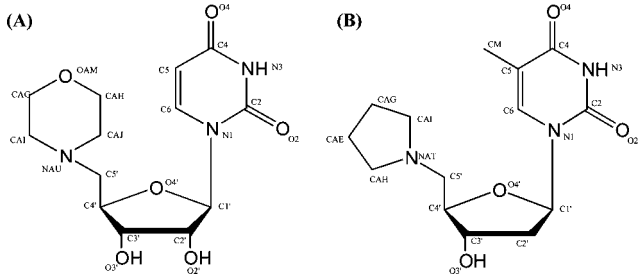

Figure 9. Chemical structure of inhibitors **U1S** and **T3S** with the numbering scheme used. The same numbering scheme was used for the other uridilyl and thymidilyl inhibitors.

concentration 0.67 mM) separately to a final volume of 100 μL, and the resulting solutions were incubated for 3 h. The 20 μL aliquots of the incubated mixtures were mixed with 20 μL of tRNA (5 mg/mL tRNA freshly dissolved in RNase free water) and incubated for another 30 min. Then 10 μL of sample buffer which consists of 10% glycerol and 0.025% bromophenol blue in RNase A free water was added to the mixture and 15 μL of it extracted and loaded onto a 1.1% agarose gel. The residual tRNA was visualized after ethidium bromide staining under UV light.

(ii) Inhibition of RNase A by compounds **U2S**−**U4S**, **T3S**, and **T4S** were assayed qualitatively by the degradation of tRNA in a comparative agarose gel. In this method, 20 μL of RNase A (stock concentration 6.29 μM) was mixed with 80 μL of the compounds **U2S**−**U4S**, **T3S**, and **T4S** (stock concentration 0.17 mM) separately, and the resulting solutions were incubated for 3 h. Then gel was run according to the method described above, and the residual tRNA was visualized after ethidium bromide staining under UV light.

(B) Precipitation Assay with RNase A. Inhibition of the ribonucleolytic activity of RNase A was quantified by the precipitation assay as described by Bond.[45] In this method 10 μL of RNase A (stock concentration 11.04 μM) was mixed with 40 μL (stock concentration 0.80 mM) of compounds **U1S**−**U4S**, **T3S**, and **T4S** to a final volume of 100 μL and incubated for 2 h at 37 °C. An amount of 20 μL of the resulting solutions from the incubated mixtures was then mixed with 40 μL of tRNA (5 mg/mL tRNA freshly dissolved in RNase A free water) and 40 μL of Tris-HCl buffer of pH 7.5 containing 5 mM EDTA and 0.5 mg/mL HSA. After incubation of the reaction mixture at 25 °C for 30 min, 200 μL of ice-cold 1.14 N perchloric acid containing 6 mM uranyl acetate was added to quench the reaction. The solution was then kept in ice for another 30 min and centrifuged at 4 °C at 12 000 rpm for 5 min. An amount of 50 μL of the supernatant was taken and diluted to 1 mL. The decrease in absorbance at 260 nm was measured and compared to that of a control set.

(C) Inhibition Kinetics with RNase A. The inhibition of RNase A by compounds **U1S**−**U4S**, **T3S**, and **T4S** was assessed individually by a spectrophotometric method as described by Anderson and co-workers.[38] The assay was performed in 0.1 M Mes-NaOH buffer, pH 6.0, containing 0.1 M NaCl using 2′,3′-cCMP as the substrate. Experiments were repeated at least three times for each set. The inhibition constants (K_i) were determined from initial velocity data. The reciprocal of initial velocity was plotted against the inhibitor concentration (Dixon plot) according to the following equation:

$$\frac{1}{v} = \frac{K_m}{V_{max}[S]K_i}[I] + \frac{1}{V_{max}}\left[1 + \frac{K_m}{[S]}\right]$$

where v is the initial velocity, [S] the substrate concentration, [I] the inhibitor concentration, K_m the Michaelis constant, K_i the inhibition constant, and V_{max} the maximum velocity.

4.3. Crystallization, Data Collection, and Structure Refinement. Bovine pancreatic RNase A (type XII-A) and other chemicals were obtained from Sigma-Aldrich (Athens, Greece). Native crystals of RNase A grown in the monoclinic lattice *C*2 as described previously[17] were soaked with compounds **U1S**, **U2S**, **U3S**, **U4S**, **T3S**, and **T4S** at a concentration of 80 mM in a buffered solution (20 mM sodium citrate, pH 5.5, 25% PEG 4000) prior to data collection. Diffraction data were collected on station PX9.6 (λ = 0.92 Å) SRS, Daresbury, U.K., at 100 K, using a ADSC CCD detector. Data were processed using the HKL package,[46] and intensities were transformed to amplitudes by the program TRUNCATE.[47] Phases were obtained using the structure of free RNase A from monoclinic crystals at 100 K as starting model.[16] Alternate cycles of manual building with the program COOT[48] and refinement using the maximum likelihood target function as implemented in the program REFMAC[49] improved the model. Inhibitor molecules were modeled using the Dundee PRODRG server (http://davapc1.bioch.dundee.ac.uk/programs/prodrg/), and they were included in the refinement procedure during its final stages. A final round of TLS (translation/libration/screw) refinement within the program REFMAC[49] using TLS groups for the protein generated by the TLSMD Web server[50] improved considerably the final model. Details of data processing and refinement statistics are provided in Supporting Information.

The program PROCHECK[51] was used to assess the quality of the final structure. Analysis of the Ramachandran ($\varphi-\psi$) plot showed that all residues lie in the allowed regions. Solvent accessible areas were calculated with the program NACCESS.[52] Figures were prepared with the program MOLSCRIPT[53] or BOBSCRIPT[54] and rendered with Raster3D.[55]

Acknowledgment. A.S. thanks the Council of Scientific and Industrial Research, New Delhi, India, for a fellowship. S.D. and T.P. thank the Department of Science and Technology (DST), New Delhi, India, for Research Grant SR/S5/OC-13/

2002. DST is also thanked for the creation of 400 MHz facility in the Department of Chemistry, Indian Institute of Technology Kharagpur, India, under the IRPHA program. D.D.L., S.E.Z., and N.G.O. thank the staff at EMBL, Hamburg, and SRS, Daresbury, U.K., for providing excellent facilities for X-ray data collection. This work was supported by the Hellenic General Secretariat for Research and Technology (GSRT), through a Joint Research and Technology project between Greece and The Czech Republic (2006−2008) (to D.D.L.), and the program "Excellence in Research Institutes (2nd cycle)" to N.G.O. EU Marie Curie Early Stage Training (EST) program (Contract No. MEST-CT-020575) (to D.D.L. and N.G.O.) is also acknowledged for support. This work was also supported by grants from European Community−Research Infrastructure Action under the FP6 "Structuring the European Research Area Programme" for work at the Synchrotron Radiation Source, CCLRC, Daresbury, U.K. (Contract No. HPRI-CT-1999-00012), and EMBL Hamburg Outstation, Germany (Contract No. RII3/CT/2004/5060008) to D.D.L and N.G.O.

Supporting Information Available: Experimental details, HPLC traces, and spectroscopic data for **U1S**, **U2S**, **T3S**, and **T4S**; Dixon plots for inhibition of RNase A by **U3S**, **U4S**, **T3S**, and **T4S**; crystallographic data collection and refinement details for compounds **U1S**−**U4S**, **T3S**, and **T4S**. This material is available free of charge via the Internet at http://pubs.acs.org.

References

(1) International; Human; Genome; Sequencing; Consortium. Finishing the euchromatic sequence of the human genome. *Nature* **2004**, *431*, 931−945.
(2) Loverix, S.; Steyaert, J. Ribonucleases: from prototypes to therapeutic targets. *Curr. Med. Chem.* **2003**, *10*, 779–785.
(3) Riordan, J. F. Angiogenin. *Methods Enzymol.* **2001**, *341*, 263–273.
(4) Rosenberg, H. F.; Domachowske, J. B. Eosinophils, eosinophil ribonucleases, and their role in host defense against respiratory virus pathogens. *J. Leukocyte Biol.* **2001**, *70*, 691–698.
(5) Rosenberg, H. F.; Domachowske, J. B. Eosinophil-derived neurotoxin. *Methods Enzymol.* **2001**, *341*, 273–286.
(6) Venge, P.; Bystrom, J.; Carlson, M.; Hakansson, L.; Karawacjzyk, M.; Peterson, C.; Seveus, L.; Trulson, A. Eosinophil cationic protein (ECP): molecular and biological properties and the use of ECP as a marker of eosinophil activation in disease. *Clin. Exp. Allergy* **1999**, *29*, 1172–1186.
(7) Yakovlev, G. I.; Mitkevich, V. A.; Makarov, A. A. Ribonuclease inhibitors. *Mol. Biol.* **2006**, *40*, 867–874.
(8) Raines, R. T. Ribonuclease A. *Chem. Rev.* **1998**, *98*, 1045–1065.
(9) Russo, A.; Acharya, K. R.; Shapiro, R. Small molecule inhibitors of RNase A and related enzymes. *Methods Enymol.* **2001**, *341*, 629–648.
(10) Leonidas, D. D.; Chavali, G. B.; Oikonomakos, N. G.; Chrysina, E. D.; Kosmopoulou, M. N.; Vlassi, M.; Frankling, C.; Acharya, K. R. High-resolution crystal structures of ribonuclease A complexed with adenylic and uridylic nucleotide inhibitors. Implications for structure-based design of ribonucleolytic inhibitors. *Protein Sci.* **2003**, *12*, 2559–2574.
(11) Jenkins, C. L.; Thiyagarajan, N.; Sweeney, R. Y.; Guy, M. P.; Kelemen, B. R.; Acharya, K. R.; Raines, R. T. Binding of non-natural 3′-nucleotides to ribonuclease A. *FEBS J.* **2005**, *272*, 744–755.
(12) Jenkins, J. L.; Shapiro, R. Identification of small-molecule inhibitors of human angiogenin and characterization of their binding interactions guided by computational docking. *Biochemistry* **2003**, *43*, 6674–6687.
(13) Russo, N.; Shapiro, R. Potent inhibition of mammalian ribonucleases by 3′,5′-pyrophosphate-linked nucleotides. *J. Biol. Chem.* **1999**, *274*, 14902–14908.
(14) Leonidas, D. D.; Shapiro, R.; Irons, L. I.; Russo, N.; Acharya, K. R. Toward rational design of ribonuclease inhibitors: high-resolution crystal structure of a ribonuclease A complex with a potent 3′,5′-pyrophosphate-linked dinucleotide inhibitor. *Biochemistry* **1999**, *38*, 10287–10297.
(15) Maiti, T. K.; Soumya, D.; Dasgupta, S.; Pathak, T. 3′-*N*-Alkylamino-3′-deoxy-ara-uridines: a new class of potential inhibitors of ribonuclease A and angiogenin. *Bioorg. Med. Chem.* **2006**, *14*, 1221–1228.
(16) Leonidas, D. D.; Maiti, T. K.; Samanta, A.; Dasgupta, S.; Pathak, T.; Zographos, S. E.; Oikonomakos, N. G. The binding of 3′-*N*-piperidine-4-carboxyl-3′-deoxy-ara-uridine to ribonuclease A in the crystal. *Bioorg. Med. Chem.* **2006**, *14*, 6055–6064.
(17) Leonidas, D. D.; Shapiro, R.; Irons, L. I.; Russo, N.; Acharya, K. R. Crystal structures of ribonuclease A complexes with 5′-diphosphoadenosine 3′-phosphate and 5′-diphosphoadenosine 2′-phosphate at 1.7 A resolution. *Biochemistry* **1997**, *36*, 5578–5588.
(18) Hatzopoulos, G. N.; Leonidas, D. D.; Kardakaris, R.; Kobe, J.; Oikonomakos, N. G. The binding of IMP to ribonuclease A. *FEBS J* **2005**, *272*, 3988–4001.
(19) Moodie, S. L.; Thornton, J. M. A study into the effects of protein binding on nucleotide conformation. *Nucleic Acids Res.* **1993**, *21*, 1369–1380.
(20) Wlodawer, A.; Miller, M.; Sjolin, L. Active site of RNase: neutron diffraction study of a complex with uridine vanadate, a transition state analog. *Proc. Natl. Acad. Sci. U.S.A.* **1983**, *80*, 3628–3631.
(21) Borkakoti, N. The active site of ribonuclease A from the crystallographic studies of ribonuclease-A−-inhibitor complexes. *Eur. J. Biochem.* **1983**, *132*, 89–94.
(22) Gilliland, G. L.; Dill, J.; Pechik, I.; Svensson, L. A.; Sjolin, L. The active site of bovine pancreatic ribonuclease: an example of solvent modulated specificity. *Protein Pept. Lett.* **1994**, *1*, 60–65.
(23) Zegers, I.; Maes, D.; Dao-Thi, M.-H.; Poortmans, F.; Palmer, R.; Wyns, L. The structures of RNase A complexed with 3′CMP and d(CpA): active site conformation and conserved water molecules. *Protein Sci.* **1994**, *31*, 2322–2339.
(24) Borkakoti, N.; Moss, D. A.; Palmer, R. A. Ribonuclease A: least squares refinement of structure at 1.45 Å resolution. *Acta Crystallogr.* **1982**, *B38*, 2210–2217.
(25) Howlin, B.; Moss, D. S.; Harris, G. W. Segmented anisotropic refinement of bovine ribonuclease A by the application of rigid-body tls model. *Acta Crystallogr.* **1989**, *A45*, 851–861.
(26) deMel, V. S. J.; Doscher, M. S.; Martin, P. D.; Edwards, B. F. P. The occupancy of two distinct conformations by active-site histidine-119 in crystals of ribonuclease is modulated by pH. *FEBS Lett.* **1994**, *349*, 155–160.
(27) Mazzarella, L.; Capasso, S.; Demasi, D.; Di'Lorenzo, G.; Mattia, C. A.; Zagari, A. Bovine seminal ribonuclease. Structure at 1.9 Å resolution. *Acta Crystallogr.* **1993**, *D49*, 389–402.
(28) Berisio, R.; Lamzin, V. S.; Sica, F.; Wilson, K. S.; Zagari, A.; Mazzarella, L. Protein titration in the crystal state. *J. Mol. Biol.* **1999**, *292*, 845–854.
(29) Fedorov, A. A.; Joseph-McCarthy, D.; Fedorov, E.; Sirakova, D.; Graf, I.; Almo, S. C. Ionic interactions in crystalline bovine pancreatic ribonuclease A. *Biochemistry* **1996**, *35*, 15962–15979.
(30) Richards, F. M.; Wyckoff, H. W. Bovine pancreatic ribonuclease. *Enzymes* **1971**, *4*, 647–806.
(31) Iwahashi, K.; Nakamura, K.; Mitsui, Y.; Ohgi, K.; Irie, M. Further evidence for the existence of the P_0 site on the active site of ribonuclease. The binding of thymidine 3′,5′-diphosphate to ribonuclease. *J. Biochem. (Tokyo)* **1981**, *90*, 1685–1690.
(32) Witzel, H.; Barnard, E. A. Mechanism and binding sites in the ribonuclease reaction II. Kinetic studies on the first step of the reaction. *Biochem. Biophys. Res. Commun.* **1962**, *7*, 295–299.
(33) Toiron, C.; Gonzalez, C.; Bruix, M.; Rico, M. Three-dimensional structure of the complexes of ribonuclease A with 2′,5′-CpA and 3′,5′-d(CpA) in aqueous solution, as obtained by NMR and restrained molecular dynamics. *Protein Sci.* **1996**, *5*, 1633–1647.
(34) Richards, F. M.; Wyckoff, H. W. Ribonuclease S. In *Atlas of Molecular Structures in Biology*; Philips, D. C., Richards, F. M., Eds.; Clarendon: Oxford, U.K., 1973; Vol. 1.
(35) Wodak, S. Y.; Liu, M. Y.; Wyckoff, H. W. The structure of cytidilyl (2′,5′) adenosine when bound to pancreatic ribonuclease S. *J. Mol. Biol.* **1977**, *116*, 855–875.
(36) Jardine, A. M.; Leonidas, D. D.; Jenkins, J. L.; Park, C.; Raines, R. T.; Acharya, K. R.; Shapiro, R. Cleavage of 3′,5′-pyrophosphate-linked dinucleotides by ribonuclease A and angiogenin. *Biochemistry* **2001**, *40*, 10262–10272.
(37) Beach, H.; Cole, R.; Gill, M. L.; Loria, J. P. Conservation of mus-ms enzyme motions in the apo- and substrate-mimicked state. *J. Am. Chem. Soc.* **2005**, *127*, 9167–9176.
(38) Anderson, D. G.; Hammes, G. G.; Walz, F. G. Binding of phosphate ligands to ribonuclease A. *Biochemistry* **1968**, *7*, 1637–1645.
(39) delCardayre, S. B.; Raines, R. T. Structural determinants of enzymatic processivity. *Biochemistry* **1994**, *33*, 6031–6037.
(40) delCardayre, S. B.; Raines, R. T. A residue to residue hydrogen bond mediates the nucleotide specificity of ribonuclease A. *J. Mol. Biol.* **1995**, *252*, 328–336.
(41) Wang, R.; Steensma, D. H.; Takaoka, Y.; Yun, J. W.; Kajimoto, T.; Wong, C. H. A search for pyrophosphate mimics for the development of substrates and inhibitors of glycosyltransferases. *Bioorg. Med. Chem.* **1997**, *5*, 661–672.
(42) Reist, E. J.; Goodman, L.; Benitez, A. Synthesis of some 5′-thiopentofuranosylpyrimidines. *J. Org. Chem.* **1964**, *29*, 554–558.

(43) Sakthivel, K.; Kumar, R. K.; Pathak, T. Reactions of dimesylthymidine with secondary-amines. Easy access to 3′,5′-dideoxy-3′-substituted-5′-alkylaminothymidines. New classes of potential antiviral amino-nucleosides. *Tetrahedron* **1993**, *49*, 4365–4372.
(44) Sela, M.; Anfinsen, C. B. Some spectrophotometric and polarimetric experiments with ribonuclease. *Biochim. Biophys. Acta* **1957**, *24*, 229–235.
(45) Bond, M. D. An in vitro binding assay for angiogenin using placental ribonuclease inhibitor. *Anal. Biochem.* **1988**, *173*, 166–173.
(46) Otwinowski, Z.; Minor, W. Processing of X-ray Diffraction Data Collected in Oscillation Mode. In *Methods in Enzymology*; Carter, C. W. J., Sweet, R. M., Eds.; Academic Press: New York, 1997; Vol. 276, pp 307−326.
(47) French, S.; Wilson, K. S. On the treatment of the negative intensity observations. *Acta Crystallogr.* **1978**, *A34*, 517–525.
(48) Emsley, P.; Cowtan, K. Coot: model-building tools for molecular graphics. *Acta Crystallogr., Sect. D: Biol. Crystallogr.* **2004**, *60*, 2126–2132.
(49) Murshudov, G. N.; Vagin, A. A.; Dodson, E. J. Refinement of macromolecular structures by the maximum-likelihood method. *Acta Crystallogr.* **1997**, *D53*, 240–255.
(50) Painter, J.; Merritt, E. A. TLSMD Web server for the generation of multi-group TLS models. *J. Appl. Crystallogr.* **2005**, *39*, 109–111.
(51) Laskowski, R. A.; MacArthur, M. W.; Moss, D. S.; Thornton, J. M. PROCHECK, a program to check the stereochemical quality of protein structures. *J. Appl. Crystallogr.* **1993**, *26*, 283–291.
(52) Hubbard, S. J.; Thornton, J. M. *NACCESS*; Department of Biochemistry and Molecular Biology, University College: London, 1993.
(53) Kraulis, P. J. MOLSCRIPT, a program to produce both detailed and schematic plots of protein structures. *J. Appl. Crystallogr.* **1991**, *24*, 946–950.
(54) Esnouf, R. M. An extensively modified version of Molscript that includes greatly enhanced coloring capabilities. *J. Mol. Graphics Modell.* **1997**, *15*, 132–134.
(55) Merritt, E. A.; Bacon, D. J. Raster3D: photorealistic molecular graphics. *Macromol. Crystallogr.* **1997**, *B277*, 505–524.
(56) McDonald, I. K.; Thornton, J. M. Satisfying hydrogen bonding potential in proteins. *J. Mol. Biol.* **1994**, *238*, 777–793.

JM800724T